TRANSACTIONS ON ELECTROMAGNETIC SPECTRUM

Multifocal THz Emission with Multiple Resonances

Tamanna Punia[1*]

[1]Department of Physics, PST Laboratory, Indian Institute of Technology, Delhi, New Delhi-110016, India
Email: tamannapunia01@gmail.com

Hitendra K. Malik[2]

[2]Department of Physics, Indian Institute of Technology, Delhi, New Delhi-110016, India
Email: hkmalik@hotmail.com

*** Corresponding author's e-mail address:** tamannapunia@gmail.com

Received: 18 March 2023
Revised: 4 April 2023
Accepted: 10 April 2023

Research Article
Vol.2 / No.2 / 2023
Doi: 10.5281/zenodo.7805204

Abstract: This analytical study shows an interesting mechanism for the emission of THz radiation due to the production of an extra transverse component of the nonlinear ponderomotive force when an external periodic electric field is applied to a plasma having density ripples. Three components of the nonlinear ponderomotive force; one due to the beating of the incident lasers and two others due to the coupling of the external electric field with the incident lasers' field are responsible for the generation of different nonlinear currents. These nonlinear currents excited at different resonances lead to the emission of multifocal THz fields. The periodicities of density ripples (β) and external electric field help in attaining the multiple resonance conditions for the emission of multiple THz fields. The amplitude of emitted THz radiation can be tuned via the magnitude of the external electric field, laser beam and plasma parameters. The magnitude of the beat wave-enabled field is 10^2 times higher than the magnitude of THz fields induced due to external electric fields.

Keywords: Ponderomotive, beating, induced, ripples.

Cite this paper as: Punia T., Malik H. K. Multifocal THz Emission with Multiple Resonances. Transactions On Electromagnetic Spectrum. 2023; 2(2): 25-32, Doi:10.5281/zenodo.7805204

1. INTRODUCTION

THz radiation gap is the gap between infrared waves and microwaves. This gap is unique because of its versatile properties, such as non-ionizing nature, penetration through opaque materials, reflection by metals and absorption by water etc. [1-2]. These radiations are not only useful in security systems, topography, agricultural industries, material science, and communication systems but also in the bio-medical fields where targeted drug delivery is required [3-6]. Despite the studies done till now, it is still a challenge to obtain tunable, efficient, convertible and multifocal THz sources. THz sources with all the features have proved to be an asset to human beings. The requirement of the high dipole moment by a medium for the transitions between the levels in the THz range is an important factor for generating highly efficient THz radiation. The inability of the electro-optic crystals, photoconductive antennas and semiconductors to fulfil this criterion limits the efficient generation of THz waves. Therefore, one of the promising mechanism for generating efficient THz radiation is the interaction between the laser and plasma, as plasma does not have any breakdown

This work is licensed under a Creative Commons Attribution 4.0 License. For more information: https://creativecommons.org/licenses/by-nc/4.0/,

limit evenfor high-intensity radiations [7]. The interaction between the laser and plasma has been explored [8]. Antonsen et al. [9] investigated the effect of density ripples on phase-matching conditions, which leads to stronger excitations in the plasma. Theoretical and experimental investigations for the efficient emission of the x-rays required for lithography were performed by Demir et al. [10]. The generation of THz radiation in the magnetized plasma has been investigated by the Nishida group [11-13]. The excitation of Cerenkov waves for THz radiation generation in the magnetized plasma using short laser pulses has been studied theoretically by Yoshii et al. [14] and experimentally by Yugami et al. [15]. A substantial increment in the efficiency of the generated THz radiation when a transverse magnetic field is applied to the medium of plasma has been shown by Wu et al. [16]. The external magnetic field has also been found to modify the electron dynamics in other nonlinear phenomena [17,18]. For efficient THz emission, different laser pulse profiles have been employed [8,19], which also contributed to other nonlinear phenomena [20-22]. The main goal of the present study is to uncover the role of skewness in pulse profile. Hence, we consider an interaction of two highly focused skew-coshyperbolic-Gaussian laser beams with preformed plasma in which an external electric field is applied. The density ripples in the plasma and the periodicity of the external static electric field play a vital role in producing multifocal THz radiation with multiple resonances.

2. MATHEMATICAL EQUATIONS

2.1. Electron oscillatory velocity and different kinds of pondermotive force

In this study, we have taken two linearly polarized skew-chG beams (SCGB's) with amplitude E_{0l}, wavenumber k_j and frequency ω_j propagating along z-direction and beat them together on a preformed plasma having density ripples. In a preformed plasma, density ripples with magnitude n_β can be written as $n' = n_\beta e^{i\beta z}$, β being the wave number. A patterned mask and trans-missive ring grating can be used for generating density ripples in which ripple parameters can be tuned by adjusting the size andperiod of the ripples. Also, another method has been proposed using microwaves [23]. The electric field of the incident SCGB's is taken as,

$$\vec{E}_{jl} = A_l \exp\left[i\left(k_j z - \omega_j t\right)\right]\hat{y} \; ; A_l = E_{0l} \cosh^m\left(\frac{ys}{a_0}\right) e^{-\left(\frac{ys}{a_0}\right)^q} \tag{1}$$

Here m, a_0, q and s are the beam order, the beam width of the laser for full-width half maximum (FWHM), laser index and skewness parameter of the beam, respectively. Eqn. (1) represents SCGB's profile for $q > 2$ and Gaussian laser profile for $q = 2$.

A spatially periodic external static electric field, $\vec{E}_p = E_{0p} e^{i(\xi_{0p} z)} \hat{y}$ with periodicity, $\xi_{0p} = \xi = \pi/a_0$ is also applied to the plasma. The polarization of the external electrostatic field is the same as that of incident lasers' electric field. Higashiguchi et al. have shown a similar spatially periodic time independent electric field so as to observe upshift in frequency from DARC [24]. In our case, we will show that both the periods may facilitate tuning of the resonance conditions via matching of the wavenumbers.

The dynamics of the plasma electrons is explained by the Drude eqn. of motion,

$$\frac{\partial v_j}{\partial t} = -\frac{e\vec{E}}{m_e} \tag{2}$$

Here, $\vec{E} = \vec{E}_{jl} + \vec{E}_p$ is the resultant field due to the incident laser field and external electric field where j = 1,2 stands for laser 1 and 2, respectively. Only the plasma electrons attain oscillatory velocity not the positive ions (due to high frequency of the laser beam), which is given by $v_j = \frac{e(\vec{E}_{jl} + \vec{E}_p)}{m_e(i\omega_j)}$. The symbol m_e represents the mass of the electron. To perform the beating process in the preformed plasma, the autofocusing of the two incident lasers is done by the optical lens placed along the z-axis. Due to the presence of the external electric field ($\vec{E}_p$), the electrons in the plasma not only experience a nonlinear ponderomotive force $(F_P^{NL})_{Beating}$ at the beating frequency but also at the modified frequency and wave numbers due to the coupling of the external electric field with the incident laser beam's electric field. The nonlinear ponderomotive force is obtained from ponderomotive potential, $\phi_p = \frac{e(\vec{E}_{1l} + \vec{E}_p).(\vec{E}_{2l} + \vec{E}_p)^*}{2m_e\,(i\omega_1)\,(i\omega_2)}$. The expression of nonlinear ponderomotive force reads

This work is licensed under a Creative Commons Attribution 4.0 License. For more information: https://creativecommons.org/licenses/by-nc/4.0/,

$$\vec{F}_p^{nl} = \frac{-e^2\vec{\nabla}\left((\vec{E}_{1l}+\vec{E}_p).(\vec{E}_{2l}+\vec{E}_p)^*\right)}{2m_e\,(i\omega_1)\,(i\omega_2)} \tag{3}$$

This force has four components as,

$$\vec{F}_p^{nl} = \frac{-e^2\vec{\nabla}(A+B+C+D)}{2m_e\,(i\omega_1)\,(i\omega_2)}, \tag{4}$$

Here $A = \vec{E}_{1l}.\vec{E}_{2l}^*$, due to the beating of two SCGB's in the plasma = $\left(F_{p1}^{nl}\right)_{Beating}$,

$B = \vec{E}_{1l}.\vec{E}_p^*$, due to the coupling of SCGB 1 and external electric field = $\left(IF_{p2}^{nl}\right)_{EF}$,

C = $\vec{E}_{2l}^*.\vec{E}_p$, due to the coupling of SCGB 2 and external electric field = $\left(IF_{p3}^{nl}\right)_{EF}$,

$D = \vec{E}_p.\vec{E}_p^*$, due to the external electric field $\vec{E}_p$. The last term D doesn't contribute to the nonlinear ponderomotive force so it can be neglected.

The expressions of the transverse components of the force are obtained as

$$\left(F_{py1}^{nl}\right)_{Beating} = \frac{-e^2E_{0l}^2 s\cosh^{2m}\left(\frac{ys}{a_0}\right)\left(2m\tanh\left(\frac{ys}{a_0}\right)-2q\left(\frac{ys}{a_0}\right)^{q-1}\right)e^{-2\left(\frac{ys}{a_0}\right)^q}e^{i(k'z-\omega t)}}{2m_e a_0(i\omega_1)\,(i\omega_2)} \tag{5}$$

$$\left(IF_{py2}^{nl}\right)_{EF} = \frac{-e^2E_{0l}E_{0p} s\cosh^{m}\left(\frac{ys}{a_0}\right)\left(m\tanh\left(\frac{ys}{a_0}\right)-q\left(\frac{ys}{a_0}\right)^{q-1}\right)e^{-\left(\frac{ys}{a_0}\right)^q}e^{i(k''z-\omega_1 t)}}{2m_e a_0(i\omega_1)\,(i\omega_2)} \tag{6}$$

$$\left(IF_{py3}^{nl}\right)_{EF} = \frac{-e^2E_{0l}E_{0p} s\cosh^{m}\left(\frac{ys}{a_0}\right)\left(m\tanh\left(\frac{ys}{a_0}\right)-q\left(\frac{ys}{a_0}\right)^{q-1}\right)e^{-\left(\frac{ys}{a_0}\right)^q}e^{i(k'''z-\omega_2 t)}}{2m_e a_0(i\omega_1)\,(i\omega_2)} \tag{7}$$

The beat wave enabled ponderomotive force (5) oscillates with frequency $\omega = \omega_1 - \omega_2$ and wavenumber $k = k_1 - k_2$ while the induced ponderomotive forces (6 and 7) oscillate with modified frequencies (ω_1, ω_2) and wavenumbers $(k'' = k_1 - \xi, k''' = -k_2 + \xi)$, respectively. The oscillations of plasma electrons become nonlinear under the effect of the nonlinear ponderomotive force.

2.2. Calculation of different types of plasma currents

The electrons attain nonlinear velocity, $v_y^{nl} = \frac{\vec{F}_p^{nl}}{m_e(-i\omega)}$ due to the nonlinear ponderomotive force experienced by them. The nonlinearity in the oscillations of electrons creates nonlinear perturbations in the density (N^{nl}) because of the redistribution of the electrons in the plasma due to which generation of space charge field of potential, ϕ and self-consistent linear perturbations in the density (N^l) occur. With the help of the continuity equation, the linear and nonlinear perturbations in density are; $N^l = -\frac{\chi_e\vec{\nabla}.\vec{\nabla}\phi}{m_e\omega_p^2}$ and $N^{nl} = -\frac{N_0\vec{\nabla}.\vec{F}_p^{nl}}{m_e\omega(\omega)}$, respectively. Taking into account the effect of both the density perturbations i.e. N^{nl} and N^l, the space charge potential ϕ can be evaluated from Poisson's eqn. $\nabla^2\phi = 4\pi\sigma\left(N^l + N^{nl}\right)$. This can be rewritten in terms of ponderomotive force as, $\vec{\nabla}\phi = \frac{\omega_p^2\vec{F}_p^{nl}}{\omega(\omega)(1+\chi_e)}$, where $\chi_e = \frac{-\omega_p^2}{\omega^2}$ is the electric susceptibility of the plasma. Therefore, the resultant transverse nonlinear velocity of electrons is calculated using the equation of motion, $\frac{\partial v_y^{nl}}{\partial t} = \frac{1}{m_e}\left(\vec{F}_p^{nl} + e\vec{\nabla}\phi\right)$ and is rewritten as, $v_y^{nl} = \frac{\vec{F}_p^{nl}\,i\omega}{m_e(\omega(\omega)-\omega_p^2)}$. Due to the nonlinear velocity of the plasma electrons, the excitation of nonlinear currents in the plasma takes place since $\vec{J}^{nl} = -\frac{1}{2}n_\beta e^{i\beta z}ev_y^{nl}$, where density ripples, $n_\beta e^{i\beta z}$ are present in the plasma. The components of the current density are given by,

This work is licensed under a Creative Commons Attribution 4.0 License. For more information: https://creativecommons.org/licenses/by-nc/4.0/,

$$\left(J_{y1}^{nl}\right)_{Beating} = \frac{-ie^3 n_\beta sRE_{0l}^2 \cosh^{2m}\left(\frac{ys}{a_0}\right)\left(2q\left(\frac{ys}{a_0}\right)^{q-1} - 2m\tanh\left(\frac{ys}{a_0}\right)\right)e^{-2\left(\frac{ys}{a_0}\right)^q} e^{i[(k+\beta)z-\omega t]}}{4m_e{}^2 a_0 (i\omega_1)\,(i\omega_2)} \tag{8}$$

$$\left(IJ_{y2}^{nl}\right)_{EF} = \frac{-ie^3 n_\beta sRE_{0l}E_{0p} \cosh^{m}\left(\frac{ys}{a_0}\right)\left(q\left(\frac{ys}{a_0}\right)^{q-1} - m\tanh\left(\frac{ys}{a_0}\right)\right)e^{-\left(\frac{ys}{a_0}\right)^q} e^{i[(k_1+\beta-\xi)z-\omega_1 t]}}{4m_e{}^2 a_0 (i\omega_1)\,(i\omega_2)} \tag{9}$$

$$\left(IJ_{y3}^{nl}\right)_{EF} = \frac{-ie^3 n_\beta sRE_{0l}E_{0p} \cosh^{m}\left(\frac{ys}{a_0}\right)\left(q\left(\frac{ys}{a_0}\right)^{q-1} - m\tanh\left(\frac{ys}{a_0}\right)\right)e^{-\left(\frac{ys}{a_0}\right)^q} e^{-i[(k_2-\beta-\xi)z-\omega_2 t]}}{4m_e{}^2 a_0 (i\omega_1)\,(i\omega_2)} \tag{10}$$

where $R = \frac{\omega}{(\omega(\omega)-\omega_p^2)}$. These components of the current densities depend upon (15) for matching of the wavenumbers to achieve the phase matching conditions for the resonant excitation of the THz fields.

2.3. Generated components of THz fields

Maxwell's equation is used to obtain the following wave equation using which THz radiation emission is evaluated.

$$-\nabla^2 \vec{E}_{THz} + \vec{\nabla}\left(\vec{\nabla}\cdot\vec{E}_{THz}\right) = -\frac{4\pi i\omega}{c^2}\vec{J}^{nl} + \frac{\omega^2}{c^2}\varepsilon\vec{E}_{THz} \tag{11}$$

We use a fast variation of the field to solve the electromagnetic equation so as to analyze the properties of emitted THz radiation. The components of the emitted THz field are obtained as,

$$(E_{0THz1})_{Beating} = \frac{2\pi\omega zie^3 n_\beta sRE_{0l}^2 \cosh^{2m}\left(\frac{ys}{a_0}\right)\left(2q\left(\frac{ys}{a_0}\right)^{q-1} - 2m\tanh\left(\frac{ys}{a_0}\right)\right)e^{-2\left(\frac{ys}{a_0}\right)^q}}{4k_{T1}c^2 m_e{}^2 a_0 (i\omega_1)\,(i\omega_2)}, \tag{12}$$

which is primary THz field due to the beating of lasers in a density rippled plasma. In addition to the primary field, two secondary fields are also emitted. The amplitude of secondary THz fields is given by,

$$(IE_{0THz2})_{EF} = \frac{2\pi\omega zie^3 n_\beta sRE_{0l}E_{0p} \cosh^{m}\left(\frac{ys}{a_0}\right)\left(q\left(\frac{ys}{a_0}\right)^{q-1} - m\tanh\left(\frac{ys}{a_0}\right)\right)e^{-\left(\frac{ys}{a_0}\right)^q}}{4k_{T2}c^2 m_e{}^2 a_0 (i\omega_1)\,(i\omega_2)}, \tag{13}$$

$$(IE_{0THz3})_{EF} = \frac{2\pi\omega zie^3 n_\beta sRE_{0l}E_{0p} \cosh^{m}\left(\frac{ys}{a_0}\right)\left(q\left(\frac{ys}{a_0}\right)^{q-1} - m\tanh\left(\frac{ys}{a_0}\right)\right)e^{-\left(\frac{ys}{a_0}\right)^q}}{4k_{T3}c^2 m_e{}^2 a_0 (i\omega_1)\,(i\omega_2)} \tag{14}$$

The phase matching conditions are obtained when $\left(k_{Ty}^2 - \frac{\omega^2}{c^2}\varepsilon\right)E_{0THzy} = 0$ where $\varepsilon = \left(1 - \frac{\omega_p^2}{\omega^2}\right)$. The following wave numbers are obtained due to phase-matching conditions for the resonant excitation of different THz radiations,

$$k_{T1} = k_1 - k_2 + \beta, k_{T2} = k_1 + \beta - \xi \text{ and } k_{T3} = -k_2 + \beta + \xi \tag{15}$$

The modified wavenumbers of the corresponding THz fields are represented by (15) which signifies that by adjusting the periodicities of ripples in the density and external electric field, resonance emission of THz fields takes place.

3. RESULTS AND DISCUSSIONS

Two SCGB's with the same amplitude E_{0l} = 6.0×10^{10} V/m and wavelengths; 7.85 μm and 8.64 μm are irradiated on the plasma medium. The plasma frequency of electrons is 2.0×10^{13} radian/s. The external periodic electric field is of the order of 2.0×10^5 V/m. The values of other parameters are: $\omega = 1.10\omega_p$, s = 0.7, a_0= 0.005 cm, $z = 10\lambda_p$, $n_\beta = 0.35n_0$ with $n_0 = 1.26 \times 10^{23}/m^3$. Fig. 1. shows the profile of the incident laser with different values of the beam order, laser index and skewness parameter.

This work is licensed under a Creative Commons Attribution 4.0 License. For more information: https://creativecommons.org/licenses/by-nc/4.0/,

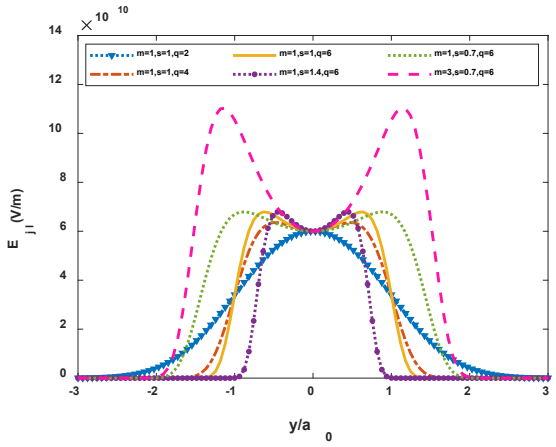

Figure 1. Distribution of the Electric field of the incident laser beam with normalized distance from beam axis for different values of the beam order, skewness parameter and laser index when b = 0.005 cm, $E_{0l} = 6.0 \times 10^{10}$V/m.

It can be observed from the Fig. 1 that for q = 2, s = 1, m = 1, the profile of the laser looks like a Gaussian and as the value of q increases from 2.0 to 4.0 and then to 6.0, a sharp gradient in the intensity of the incident laser beam can be seen. Also, a dip starts coming in the peaks, and two peaks are easily distinguishable. This dip in the peaks of the incident laser beam can be further controlled by the skewness parameter (s) of the laser beam. For q = 6, the distance between the peaks is inversely proportional to the value of s. For example: when m = 1, s = 0.7, q = 6, the peaks are apart, but as the value of s increases to 1, the peaks start coming closer, and when s is further increased to 1.4 (keeping all the other parameters same), the peaks come much closer to each other. It can also be observed that higher beam order i.e. m = 3 results in higher amplitude peaks i.e. amplitude of the electric field increases to a new scale (order $10^{11} V/m$) when m = 3 due to sharpest gradient in the intensity of the laser beam.

Fig. 2 shows the magnitude of both the beat wave enabled and induced pondermotive forces with normalized distance from the beam axis. The magnitude of both forces i.e. $\left(F_{py}^{nl}\right)_{Beating}$ and $\left(IF_{py}^{nl}\right)_{EF}$ are plotted for q = 6 and m = 3 since the higher value of the laser index and beam order results in the stronger pondermotive force (Fig. 1). The two forces are similar in nature i.e. oscillating and symmetric about the axis of propagation. However, the magnitude of the induced ponderomotive force is 10^6 dynes smaller than the beat wave-enabled ponderomotive force. The beating force oscillates with frequency, $\omega = \omega_1 - \omega_2$ and wavenumber, $k = k_1 - k_2$ while the induced forces oscillate with a modified frequency (ω_1, ω_2) and wavenumbers (k'', k'''), respectively.

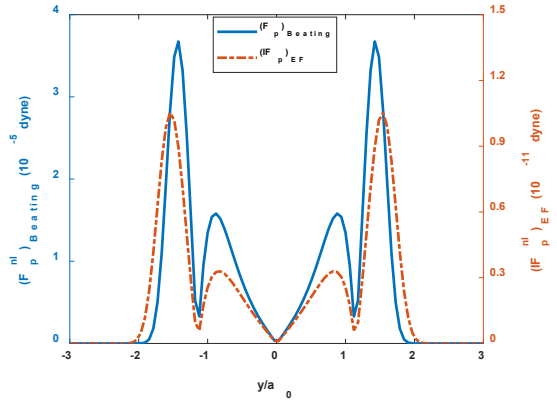

Figure 2. Distribution of the transverse component of the beat wave enabled and induced ponderomotive force with normalized distance from beam axis when a_0= 0.005 cm, q = 6, s = 0.7, $n_\beta = 0.35 n_0, \omega = 1.10 \omega_p$ and m = 3.

The peaks of these forces are located at different positions i.e. the smaller and higher amplitude peaks of the beat wave-enabled ponderomotive force occurs at $y/a_0 = 0.878$ and $y/a_0 = 1.424$ on both sides of the origin, respectively, while for the induced pondermotive force they occur at $y/a_0 = 0.818$ and $y/a_0 = 1.545$, respectively. The two peaks of either force are responsible for the bifocal emission of the THz radiation, which can be converted into unifocal emission based on the value of q (see Fig. 1). The excitation of these forces leads to the generation of nonlinear plasma currents. During the study, we are interested in exploring the

This work is licensed under a Creative Commons Attribution 4.0 License. For more information: https://creativecommons.org/licenses/by-nc/4.0/,

behaviour of induced plasma currents i.e. $\left(IJ_{py}^{nl}\right)_{EF}$ concerning to the parameters of the laser beam, electric field and plasma. So, we plot the plasma currents with normalized distance from the beam axis in Fig. 3.

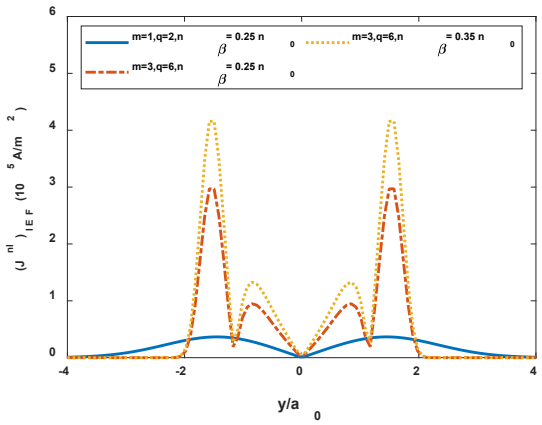

Figure 3. Distribution of the transverse induced plasma currents with normalized distance from beam axis for different values of m, q and density ripples when s = 0.7, $n_\beta = 0.35n_0$, $\omega = 1.10\omega_p$.

It can be observed that the nonlinear currents generated are oscillatory and symmetric in nature. They are higher in magnitude when laser beams of higher order and higher laser index are employed to the plasma medium. These observations are similar to the results of Fig. 1. The induced plasma currents also become stronger in amplitude on increasing the magnitude of density ripples in the plasma. The distance between the ripples should be less i.e. they should be formed at closer distances in order to achieve THz radiation emission of stronger intensity.

3.1. Comparative study of $(E_{0THz1})_{Beating}$ and $(IE_{0THz2})_{EF}$

Figures 4(a) and 4(b) make a comparative study of both the THz fields i.e. due to the beating process i.e. $(E_{0THz1})_{Beating}$ and due to the coupling process, $(IE_{0THz2})_{EF}$. It can be seen that both the fields are found to be amplified if the lasers of smaller beam width are used in the mechanism since beam width is an important parameter, and slight modifications in its values result in significant changes in the properties of the beam and hence in the ponderomotive force. For instance, the lower value of beam width leads to the production of greater ponderomotive force due to the huge increment in the gradient of the intensity of the laser beam which results in the generation of greater nonlinear currents hence, THz radiations of stronger intensity are emitted. The decay in the induced THz amplitude on increasing the beam width can be compensated by employing a laser index of higher values i.e. q = 6.

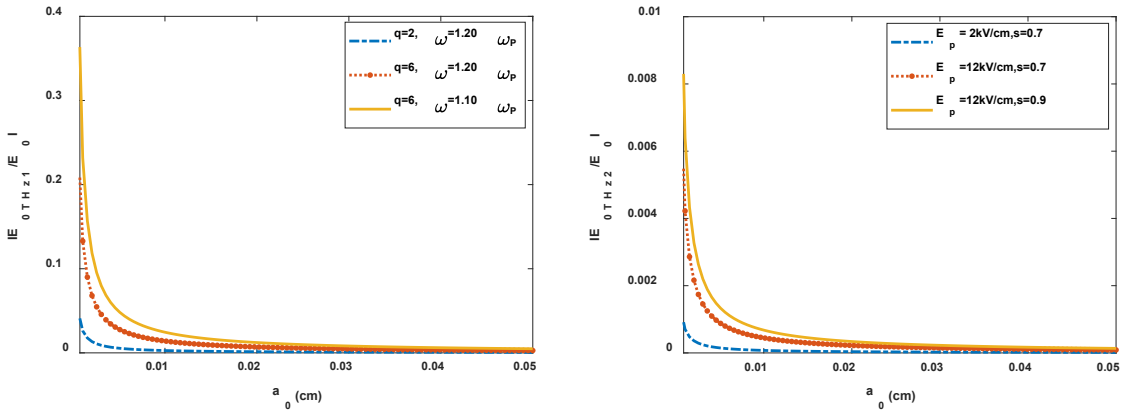

(a) (b)

Figure 4. Distribution of y-component of $(E_{0THz1})_{Beating} - (a)$ and $(IE_{0THz2})_{EF} - (b)$ with beam width when $n_\beta = 0.35n_0$ and s = 0.7.

This work is licensed under a Creative Commons Attribution 4.0 License. For more information: https://creativecommons.org/licenses/by-nc/4.0/,

In Fig. 4(a), the THz amplitude is found to be reduced when the beating frequency is away from the resonance condition i.e. $\omega = \omega_p$. So, the beating frequency should be closer to the plasma frequency in order to achieve THz radiations of stronger intensity. The induced THz field $(IE_{0THz2})_{EF}$ increases with the increase in the magnitude of the external electric field ($\vec{E}_p$) and skewness parameter, as shown in Fig. 4(b). For example, the amplitude increases to higher orders if the external electric field's magnitude increases from 2 kV/cm to 12 kV/cm. Hence, the skewness parameter not only tunes the dip in the peaks (Fig. 1.) but also controls the amplitude of emitted THz fields. The results obtained in Figs. 2, 4(a), and 4(b) agrees with the results obtained in [25] while the trend observed in Figs. 1 and 3 is similar to the trend in the studies [26,27].

4. CONCLUSIONS

An interesting mechanism for the resonant excitation of THz fields has been proposed that leads to multifocal THz emission. An additional transverse component of force is produced due to the application of an external electric field to the plasma having density ripples. For the resonant excitation of the THz fields, the tuning of the parameters ξ and β helps in achieving the phase-matching conditions. The behaviour of induced THz fields is similar to that of the beating field, however, the magnitude is smaller by order $10^2\ V/m$ for the parameters used in this study. The amplitude of the induced THz field is further explored for different parameters of a laser beam, external electric field and plasma. We conclude that induced THz radiations of stronger intensity are emitted by employing lower beam width, higher index lasers and density ripples constructed at smaller distances. The emitted multiple radiations are multifocal and convertible, hence are useful in the diagnosis and treatment of cancerous diseases. Such a conversion is possible based on the skewness in the laser's pulse profile.

Acknowledgment

The author Tamanna Punia acknowledges University Grant Commission (UGC), Government of India for providing financial support (Student ID: 1452/NOV2017-525455).

REFERENCES

[1] P. H. Siegel, Terahertz technology, IEEE Trans. Microw. Theory Tech., vol. 50, no. 3, pp. 910–928, 2002.

[2] X. He, G. Xiao, F. Liu, F. Lin, and W. Shi, Flexible properties of THz graphene bowtie metamaterials structures, Opt. Mater. Express, vol. 9, no. 1, p. 44, 2019.

[3] F. Sizov, THz radiation sensors, Opto-electronics Rev., vol. 18, no. 1, pp. 10–36, 2010.

[4] B. Ferguson and X. Zhang, Nmat708, vol. 1, no. September, pp. 1–8, 2002.

[5] D. Dragoman and M. Dragoman, Terahertz fields and applications, Prog. Quantum Electron., vol. 28, no. 1, pp. 1–66, 2004.

[6] P. Knobloch et al., Medical THz imaging: an investigation of histo-pathological samples, Physics in Medicine & Biology, vol. 47, no. 21, pp. 3875, 2002.

[7] W. P. Leemans et al., Terahertz radiation from laser accelerated electron bunches, Phys. Plasmas, vol. 11, no. 5 PART 2, pp. 2899–2906, 2004.

[8] H. K. Malik, Laser-Matter Interaction for Radiation and Energy. CRC Press, 2021.

[9] T. M. Antonsen, J. Palastro, and H. M. Milchberg, Excitation of terahertz radiation by laser pulses in nonuniform plasma channels, Phys. Plasmas, vol. 14, no. 3, pp. 1–9, 2007.

[10] P. Demir, P. Demir, E. Kacar, S. K. Bilikmen, and A. Demir, Conversion efficiency calculations for soft x-rays emitted from tin plasma for lithography applications, Springer Proc. Phys., vol. 130, pp. 281–287, 2009.

This work is licensed under a Creative Commons Attribution 4.0 License. For more information: https://creativecommons.org/licenses/by-nc/4.0/, www.tesjournal.com

[11] D. Dorranian, M. Ghoranneviss, M. Starodubtsev, H. Ito, N. Yugami, and Y. Nishida, Generation of short pulse radiation from magnetized wake in gas-jet plasma and laser interaction, Phys. Lett. Sect. A Gen. At. Solid State Phys., vol. 331, no. 1–2, pp. 77–83, 2004.

[12] D. Dorrantan, M. Ghoranneviss, M. Starodubtsev, N. Yugami, and Y. Nishida, Microwave emission from TW-100 fs laser irradiation of gas jet, Laser Part. Beams, vol. 23, no. 4, pp. 583–596, 2005.

[13] Y. Nishida and T. Shinozaki, Resonant wave-particle interactions in vp×B acceleration scheme, Phys. Rev. Lett., vol. 65, no. 19, pp. 2386–2389, 1990.

[14] J. Yoshii, C. H. Lai, T. Katsouleas, C. Joshi, and M. B. Mori, Radiation from cerenkov wakes in a magnetized plasma, Phys. Rev. Lett., vol. 79, no. 21, pp. 4194–4197, 1997.

[15] N. Yugami et al., Experimental observation of radiation from Cherenkov wakes in a magnetized plasma, Phys. Rev. Lett., vol. 89, no. 6, pp. 065003/1-065003/4, 2002.

[16] H. C. Wu, Z. M. Sheng, Q. L. Dong, H. Xu, and J. Zhang, Powerful terahertz emission from laser wakefields in inhomogeneous magnetized plasmas, Phys. Rev. E - Stat. Nonlinear, Soft Matter Phys., vol. 75, no. 1, pp. 1–7, 2007.

[17] L. Malik, M. Kumar and I.V. Singh, A Three-Coil Setup for Controlled Divergence in Magnetic Nozzle, IEEE Trans. Plasma Sci., vol. 49, no. 7 pp. 2227–2237, 2021.

[18] L. Malik, Tapered coils system for space propulsion with enhanced thrust: a concept of plasma detachment, Propulsion and Power Research, vol. 11, no. 2, pp. 171-180, 2022.

[19] H. K. Malik, Generalized treatment of skew-cosh-Gaussian lasers for bifocal terahertz radiation, Physics Letters A, vol. 384, no. 15, pp. 126304, 2020.

[20] L. Malik and A. Escarguel, Role of the temporal profile of femtosecond lasers of two different colours in holography, EPL (Europhysics Letters), vol. 124, no. 6, pp. 64002, 2019.

[21] L. Malik, Dark hollow lasers may be better candidates for holography, Optics & Laser Technology, vol. 132, pp. 106485, 2020.

[22] L. Malik, A. Escarguel, M. Kumar, A. Tevatia, and R. S. Sirohi, Uncovering the remarkable contribution of lasers peak intensity region in holography, Laser Physics Letters, vol. 18, no. 8, pp. 086003, 2021.

[23] H. K. Malik, Density bunch formation by microwave in a plasma-filled cylindrical waveguide, EPL (Europhysics Letters), vol. 106, no. 5, pp. 55002, 2014.

[24] T. Higashiguchi et al., Experimental observation of further frequency upshift from dc to ac radiation converter with perpendicular dc magnetic field, Phys. Rev. Lett., vol. 85, no. 21, pp. 4542–4545, 2000.

[25] D. Singh and H. K. Malik, Terahertz emission by multiple resonances under external periodic electrostatic field, Phys. Rev. E, vol. 101, no. 4, p. 43207, 2020.

[26] T. Punia, D. Sharma, H.K. Malik, THz Radiation Generation Through Graphite Nanoparticles Having Two Different Shapes and Orientations of Basal Planes, IEEE Trans. Plasma Sci., vol. 50, no. 4, pp. 1087–1096, 2022.

[27] H. K. Malik, T. Punia, Hat-Top Beams for Generating Tunable THz Radiations Using a Medium of Conducting Nanocylinders, Electronics, vol. 10, no. 24, pp. 3134, 2021.

This work is licensed under a Creative Commons Attribution 4.0 License. For more information: https://creativecommons.org/licenses/by-nc/4.0/,